Stable single-wavelength emission from fully chaotic microcavity lasers

Satoshi Sunada,[1] Takehiro Fukushima,[2] Susumu Shinohara,[3] Takahisa Harayama,[3,4] and Masaaki Adachi[1]

[1]*Faculty of Mechanical Engineering, Institute of Science and Engineering, Kanazawa University, Kakuma-machi Kanazawa Ishikawa 920-1192, Japan*

[2]*Department of Information and Communication Engineering, Okayama Prefectural University, 111 Kuboki Soja Okayama 719-1197, Japan*

[3]*NTT Communication Science Laboratories, NTT Corporation, 2-4 Hikaridai Seika-cho Soraku-gun, Kyoto 619-0237, Japan*

[4]*Department of Mechanical Engineering, Toyo University, 2100 Kujirai Kawagoe Saitama 350-8585, Japan*

(Received 24 January 2013; published 3 July 2013)

We experimentally and numerically show that single-wavelength emission can be stably observed for a fully chaotic microcavity laser with a stadium shape under continuous wave condition. The emission pattern is asymmetric with respect to the symmetry axes of the laser cavity, and it cannot be explained by a single cavity mode. On the basis of numerical analysis, we interpret such a lasing as the result of frequency-locking interaction among several low-loss cavity modes. Moreover, we experimentally investigate the optical spectral properties of the laser under pulsed-pumping condition, and discuss the pulse-width dependence on the number of lasing modes.

DOI: 10.1103/PhysRevA.88.013802 PACS number(s): 42.55.Sa, 42.65.Sf, 05.45.Mt

I. INTRODUCTION

Unlike one-dimensional laser cavities, such as Fabry-Perot cavities, two-dimensional (2D) laser cavities can exhibit a rich variety of lasing modes depending on the geometries of the cavity shapes [1]. Up to now, various geometries of 2D laser cavities have been proposed and investigated extensively, e.g., microdisk [2], deformed disk [3,4], spiral [5], limaçon [6], and so on. The interest in such laser devices comes from the potential applications in optical engineering [7] as well as from the viewpoint of fundamental laser physics and classical and quantum chaos theory [1,8].

In the fundamental viewpoint, fully chaotic cavities (i.e., cavities having fully chaotic ray dynamics in a ray optics picture) are of particular interest, one of whose representative examples is the stadium-shaped cavity shown in Fig. 1. Such cavities offer a good experimental stage for addressing fundamental problems regarding ray-wave correspondence in open systems [9–12] and light-matter interaction. Up to now, many theoretical and numerical studies on the lasing in fully chaotic cavities with a stadium shape have been intensively performed [13–17], where the lasing properties have been discussed based on a nonlinear dynamical model taking into account light-matter interaction.

The lasing in stadium-shaped cavities has been experimentally studied mainly under pulsed-pumping conditions [18–24]. In these studies, multimode lasing has been often observed. In contrast, only a limited number of studies are carried out with continuous wave (cw) pumping condition for chaotic cavities with other shapes [25–27]. Interestingly, it has been reported that single-mode lasing can be observed even when the cavity size is much larger than the lasing wavelength.

It would be interesting to understand the lasing property from the viewpoint of modal interactions because there exist spatially complex modes in chaotic cavities, which can lead to strong interactions via the spatial overlap. Recently, the relationship between the modal structure and the interactions has been well discussed, and it has been shown that modal interactions play an important role in so-called complex lasers such as random lasers [28,29]. At present, in fully-chaotic cavity lasers, it is unclear how modal interactions influence the lasing properties, especially the single-mode lasing property under cw condition, and how the lasing state depends on the operating condition.

In this paper, we experimentally and numerically study the lasing properties in a stadium-shaped cavity under both cw and pulsed-pumping conditions. First, it is shown that a stable single-wavelength emission can be achieved under cw pumping operation. The emission pattern is asymmetric with respect to the symmetry axes of the stadium-shaped cavity, and it does not correspond to any emission patterns of the cavity modes, although the single-wavelength lasing in other chaotic cavities reported in Refs. [25–27] have been explained on the basis of a single low-loss cavity mode. Our numerical analysis suggests that single-wavelength lasing with an asymmetric emission pattern can be interpreted as due to frequency-locking interaction among several low-loss modes. We show that owing to the interaction, several modes are integrated into a single lasing mode with a spatially extended pattern over the interior of the cavity, and the lasing mode strongly suppresses the lasing of the other modes via the spatial overlap.

In addition, we experimentally investigate how the single-wavelength lasing state is changed under the pulsed-pumping condition. We discuss the operating condition required for observing the single-wavelength lasing state and the dynamics of the modal interactions toward the lasing state.

The rest of this paper is organized as follows: In Sec. II, we report the numerical results regarding the dynamical behavior and the emission pattern of a stadium-shaped cavity laser, which are obtained by using a nonlinear dynamical model. We discuss the mechanism of the emergence of single-wavelength lasing with an asymmetric emission pattern. In Sec. III, we experimentally investigate the optical spectra and far-field pattern of a semiconductor laser diode with a stadium-shaped cavity operated under cw condition, and we demonstrate that such single-wavelength lasing can be obtained in the laser diode. In Sec. V, we report the experimental results on the lasing phenomena under pulsed-pumping conditions, and we discuss the operating condition for the single-wavelength

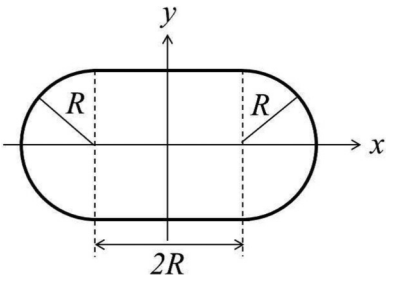

FIG. 1. A stadium-shaped cavity.

lasing and the transient dynamics toward the lasing state. Finally, Sec. IV provides a summary and discussion.

II. NUMERICAL SIMULATIONS

A. Nonlinear dynamical model

First, let us briefly introduce a nonlinear dynamical model for 2D cavities, the Schrödinger-Bloch (SB) model [16], which describes the dynamics of the slowly varying envelope of the electric field $\tilde{E}$, the polarization field $\tilde{\rho}$, and the population inversion component W in a two-level active medium:

$$\frac{\partial \tilde{E}}{\partial t} = \frac{i}{2}\left(\nabla_{xy}^2 + \frac{n^2}{n_{\text{in}}^2}\right)\tilde{E} - \alpha_L(x,y)\tilde{E} + \mu\tilde{\rho}, \tag{1}$$

$$\frac{\partial \tilde{\rho}}{\partial t} = -\tilde{\gamma}_\perp\tilde{\rho} + \tilde{\kappa}W\tilde{E}, \tag{2}$$

$$\frac{\partial W}{\partial t} = -\tilde{\gamma}_\parallel(W - W_\infty) - 2\tilde{\kappa}(\tilde{E}\tilde{\rho}^* + \tilde{E}^*\tilde{\rho}), \tag{3}$$

where space and time are made dimensionless by the scale transformation $(n_{\text{in}}\omega_0 x/c,\ n_{\text{in}}\omega_0 y/c) \to (x,y)$ and $t\omega_0 \to t$, respectively. ω_0 denotes the transition frequency of the two-level medium. The refractive index $n(x,y)$ equals n_{in} inside the cavity and n_{out} outside the cavity. $\alpha_L(x,y)$ denotes the linear absorption coefficient, which is equal to the constant α_L inside the cavity and zero outside the cavity. The two dimensionless relaxation parameters $\tilde{\gamma}_\perp$ and $\tilde{\gamma}_\parallel$ denote the transversal relaxation rate and the longitudinal relaxation rate, respectively. W_∞ and $\tilde{\kappa}$ denote the external pumping parameter and the dimensionless coupling strength, respectively.

A key to the understanding of the lasing state is the cavity modes, which are determined by the cavity shape and the refractive index. They are obtained from the wave equation (1) by omitting the polarization ρ and absorption α_L and assuming that a mode oscillates with frequency ξ_j as $\tilde{E}_j = \psi_j(\boldsymbol{r})e^{-i\xi_j t}$, where j denotes a mode number. Because of the scale transformation, the relation between ξ_j and the actual frequency ω_j is given by $\xi_j = \omega_j/\omega_0 - 1$. It is to be noted that the values of ξ_j are always complex values due to leakage from the cavity. The real part of ξ_j represents the resonant frequency, while the imaginary part represents the decay rate.

The lasing possibility of such cavity modes can be predicted as follows. In the linear limit where the nonlinearity of Eqs. (1)–(3) is omitted, the net lasing gain $g(\xi_j)$ for mode j can be obtained as the first-order correction of the imaginary part of the resonance frequency due to the presence of α_L and the active medium [16],

$$g(\xi_j) = \frac{\alpha_0\tilde{\gamma}_\perp^2}{\tilde{\gamma}_\perp^2 + \text{Re}\,\xi_j^2} + \text{Im}\,\xi_j - \alpha_L, \tag{4}$$

where $\alpha_0 = \mu\tilde{\kappa}W_\infty/\tilde{\gamma}_\perp$. In the above equation, the first term denotes a Lorentzian-shaped gain that has a maximum at $\text{Re}\,\xi_j = 0$, corresponding to the transition frequency ω_0. The second and third terms represent the cavity loss. When mode j has a positive net gain $g(\xi_j) > 0$, i.e., the gain (of the first term) exceeds the total cavity loss, the mode has a possibility to lase. However, we need to keep in mind that the linear description is correct only when the light intensity is sufficiently low.

When the cavity size is large and many modes can have positive net gain, the linear description becomes less effective, because nonlinear interaction occurs among many modes via the active medium. In particular, the modes of stadium-shaped cavities can have chaotic spatial patterns, inducing complex interaction among them [15].

In what follows, we focus on the lasing of a stadium-shaped cavity in the case where many modes can have positive net gain. From the numerical simulation of Eqs. (1)–(3) taking into account full nonlinearity, we observe that as a result of complex interaction among the modes, the cavities can exhibit a strong tendency toward a stationary stable lasing state with a single frequency.

B. Results

In our simulation, we chose a stadium which consists of two half circles of radius $R = 49/\sqrt{2}$ and two flat lines of length $2R$, as shown in Fig. 1. The refractive indices inside and outside the cavity are $n_{\text{in}} = 2$ and $n_{\text{out}} = 1$, respectively. If the lasing wavelength is assumed to be 0.85 μm, the actual radius of the stadium corresponds to 2.34 μm. Figure 2 displays the distribution of the resonances ξ of the stadium, which were calculated by using the extended boundary element method [30]. The other parameters were set as follows: $\tilde{\gamma}_\parallel = 0.003$, $\tilde{\gamma}_\perp = 0.006$, $\epsilon = 4.0$, $\alpha_L = 0.004$, $\mu = \pi/2$, $\tilde{\kappa} = 0.5$, and $W_\infty = 2 \times 10^{-3}$. For the choice of the parameter values, the modes corresponding to resonances inside the light blue region of Fig. 2 have positive net gain.

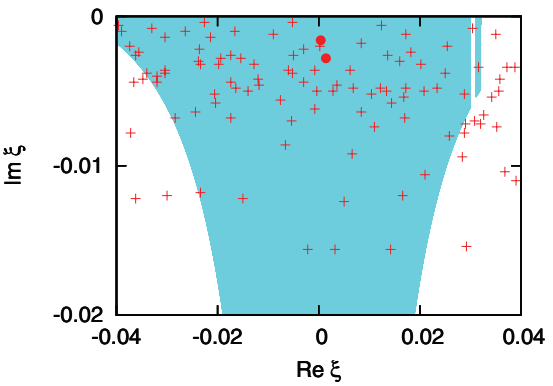

FIG. 2. (Color online) Resonances of the stadium-shaped cavity (crosses and closed circles). The resonances inside the light blue region satisfy the lasing condition $g(\xi_j) > 0$ [see Eq. (4)]. The two closed circles denote the resonances of the cavity modes dominant in the final lasing states.

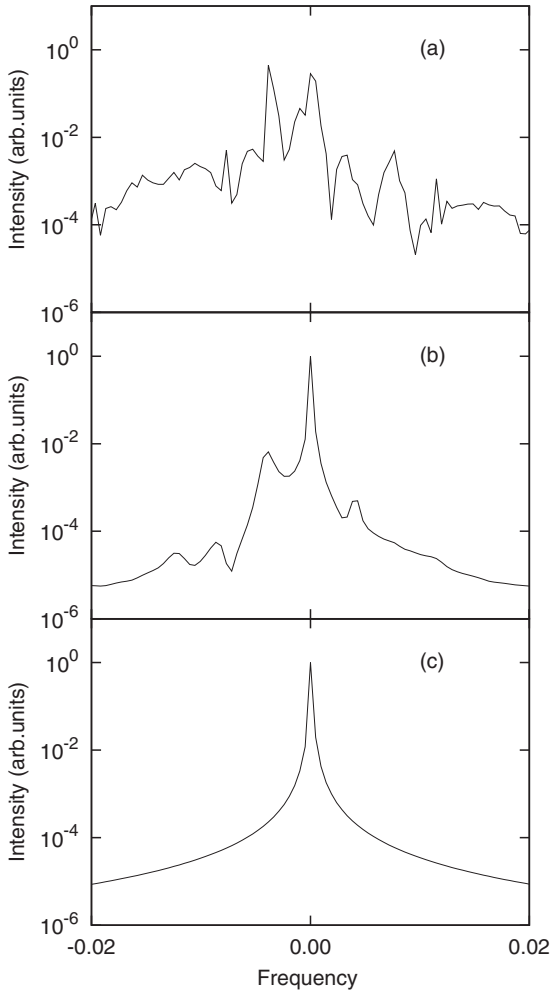

FIG. 3. Power spectra calculated from the time-series of the light-field $\tilde{E}(t)$ in three time regime, (a) $t_0(=0) < t < t_1$, (b) $t_1 \leqslant t < t_2$, and (c) $t_2 \leqslant t < t_3$.

The numerical integrations of the SB model were carried out by using the symplectic integrator method for Eq. (1) and the Euler method for Eqs. (2) and (3) [31]. The time evolution of the light field was started from an initial state of small amplitude. We observed that the initial light field first increases exponentially, and after a relaxation process, a stationary lasing state is realized, where the light intensity saturates to a constant value.

1. *Time dependence of spectrum*

An interesting dynamical behavior can be seen in a transient time regime toward the stationary final lasing state. Figure 3 shows the time dependence of the optical spectrum. The spectra are calculated from the time series of the light field $\tilde{E}(t)$ in three time regimes. Each time regime is set such that $t_{j-1} \leqslant t < t_j$ $(j = 1,2,3)$, where $t_j = j \times t_1$, and $t_0 = 0$ and t_3 ($\approx$50 000) denote an initial time when the laser action starts and a time after relaxation to the stationary lasing state, respectively. The power spectrum of the first time regime is shown in Fig. 3(a). The spectrum shows several peaks around $\xi = 0$ (i.e., the gain center of the active medium), which correspond to the modes satisfying the linear lasing condition (4). In the second regime, the peak closest to the gain center gets larger, while the other peaks are suppressed as the result of gain competition [Fig. 3(b)]. For the power spectrum of the third regime [Fig. 3(c)], we can identify only one peak, whose interpretation will be given later.

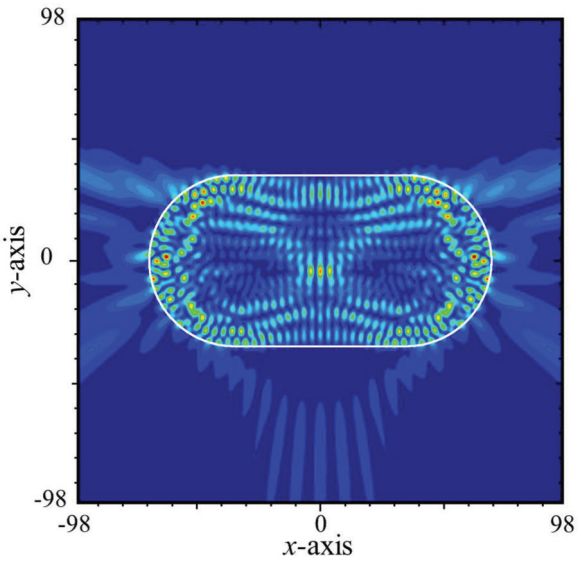

FIG. 4. (Color online) Spatial intensity pattern of the stationary lasing mode. The white curve defines the stadium-shaped cavity.

2. *Spatial pattern*

Next, we investigated the spatial pattern of the stationary single-frequency lasing state. Figure 4 shows its spatial pattern, which reveals that the pattern is asymmetric with respect to the x axis, while it is symmetric with respect to the y axis. Since the spatial patterns of cavity modes are symmetric with respect to both the x and y axes due to the symmetry of the stadium shape (e.g., see Fig. 5), the asymmetric pattern cannot be simply attributed to a single cavity mode.

According to Refs. [14–16], the generation of the asymmetric pattern can be explained by the frequency-locking phenomena among cavity modes with different parities. Here, let $\psi(x,y)$ be the wave function of the cavity modes. Due to the symmetry of the stadium shape, the wave functions are divided into four symmetry classes $\psi_{ab}(-x,y) = a\psi_{ab}(x,y)$ and $\psi_{ab}(x,-y) = b\psi_{ab}(x,y)$ with the parities $a \in (+,-)$ and $b \in (+,-)$, respectively. If the resonant frequencies of the cavity modes with different parities are close to each other, they can lase simultaneously, and for sufficiently strong interactions their frequencies are locked so that the difference in the frequency becomes zero. The interference among the lasing modes with the same frequency but with different parities can lead to an asymmetric pattern.

Our numerical analysis based on cavity-mode calculation and a linear stability analysis reveals that the cavity modes of the resonances denoted by the closed circles in Fig. 2 have parities $(+.+)$ and $(-,+)$, as shown in Fig. 5, and they can have a large net gain due to the low loss. Since their frequencies are close to each other (i.e., they are nearly degenerate) and there is a spatial overlap between the two modes [32], the frequency-locking interaction is easily caused between them,

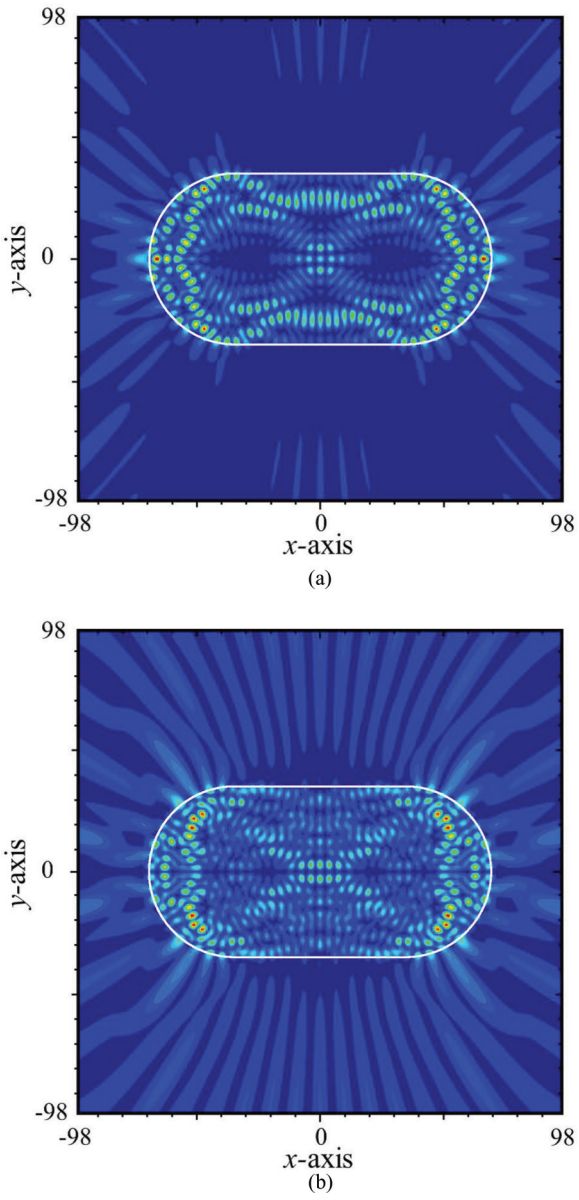

FIG. 5. (Color online) Spatial intensity patterns of the cavity modes corresponding to the resonances of (a) the left circle and (b) the right circle in Fig. 2. The symmetry classes of these modes are, respectively, (a) even-even, $\psi_{++}(x,y)$ and (b) odd-even, $\psi_{-+}(x,y)$. Since the intensity pattern has a node (an antinode) along the x (y) axis [$y = 0$ ($x = 0$)], the pattern has odd (even) symmetry with respect to the x (y) axis. The white curve defines the stadium-shaped cavity.

and the asymmetric pattern with respect to the x axis can be generated by the interference between them.

We note that the lasing pattern that is the reverse of that shown in Fig. 4 with respect to the x axis is also a stable lasing state with the same frequency. Which lasing pattern appears depends on the initial states of the light field and the active medium. The bistability of the lasing pattern is a property seen in 2D cavity lasers with an axial symmetry, such as stadium lasers [14].

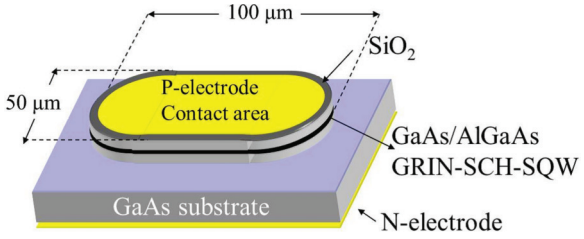

FIG. 6. (Color online) The schematic of the stadium-shaped semiconductor laser diode.

3. Discussion on single-frequency lasing

Lastly in this section, we discuss the mode selection process to the stable single-frequency lasing state. Because the gain competition occurs for the modes sharing a common population inversion, the spatial patterns of cavity modes play a crucial role in the competition. In the stadium-shaped cavity, a mode typically has a complex pattern spread over the cavity, so that the population inversion is almost uniformly depleted by the modes within the gain band, and the overlaps of these modes lead to strong modal interactions among them. Previous simulations of the SB model for stadium-shaped cavity lasers show that only a few modes can lase, even when many modes have positive net gain [15]. The tendency becomes more prominent as the pumping power increases. Such strong mode selection can also be seen in the other homogeneously broadening lasers with spatially complex modes [33]. Moreover, in our simulations, the frequency-locking interaction also plays an important role: The interaction integrates the two modes shown in Fig. 5 into a single lasing mode, and can further extend the spatial distribution to the whole cavity, as shown in Fig. 4. Consequently, the lasing mode can deplete the population inversion more uniformly, thereby preventing the other modes from being excited.

For larger cavities, the spatial patterns of the cavity modes become more complex. Moreover, the spacing between the neighboring resonant frequencies becomes smaller, which will make it easier to cause the frequency-locking interaction. Therefore, it can be expected that single-frequency lasing can be easily achieved even in large-sized cavities. In the next section, we experimentally verify this with a stadium-shaped semiconductor laser diode.

III. LASING PROPERTIES UNDER cw PUMPING CONDITION

A. Stadium-shaped semiconductor laser diode

Figure 6 shows the schematic structure of the laser diode used in the experiment. The radius R of the two half circles is 25 μm, and the length of the straight segments is 50 μm, which is about 11 times larger than the stadium-shaped cavity studied numerically in the previous section. The laser diode was fabricated by applying a reactive-ion-etching technique to a graded index separate confinement heterostructure (GRIN-SCH) single quantum well GaAs/AlGaAs structure that was grown by metal-organic chemical-vapor deposition. The details of the layer structure and fabrication process are similar to those reported in [18]. The laser was soldered on an AlN (aluminum nitride) submount with high thermal conductivity,

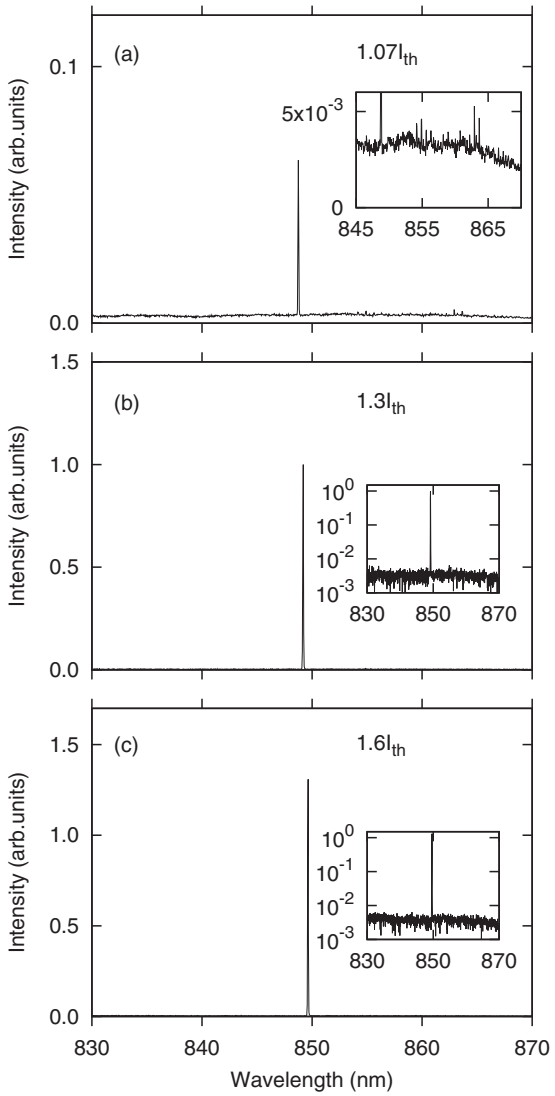

FIG. 7. Optical spectra obtained for injection current values of (a) $1.07I_{\text{th}}$, (b) $1.3I_{\text{th}}$, and (c) $1.6I_{\text{th}}$. The inset in (a) shows the enlargement around the wavelength of 855 nm. The insets in (b) and (c) show the corresponding logarithmic scale plots, clearly showing the nonexistence of side peaks.

and the temperature was maintained at 25 °C. The optical output was collected from the major axis of the stadium using two antireflection coated lenses. One lens was used to collect light from the laser, while the other one was used to refocus it onto a multimode optical fiber. The collection efficiency was ~5.9%, which is sufficient to evaluate the lasing properties.

B. Optical and rf spectra

Under cw condition, the lasing action was confirmed by the appearance of sharp narrow peaks in the optical spectrum when the injection current to the laser diode was increased above 75 mA ($=I_{\text{th}}$). Figures 7(a)–7(c) show the optical spectra obtained for various values of the injection current. The position of the dominant peak is found to be close to the maximum value of the amplified spontaneous emission (ASE) spectrum measured below the threshold current. As shown in Fig. 7(a) and its inset, the multiple peaks appear just above

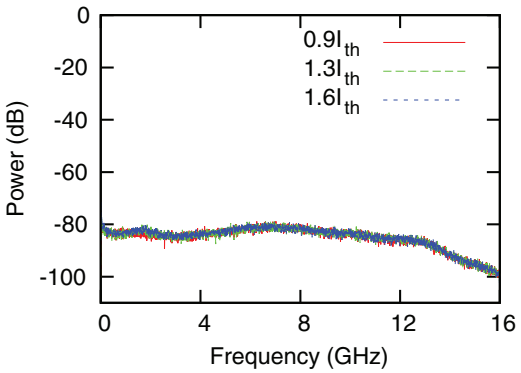

FIG. 8. (Color online) rf spectra for the injection current values of $0.9I_{\text{th}}$, $1.3I_{\text{th}}$, and $1.6I_{\text{th}}$, which are almost on top of each other.

the threshold. However, as the injection current increases, the dominant peak increases while the intensities of the other peaks decrease. For the injection current above $\approx 1.3\ I_{\text{th}}$, we can observe a single peak in the optical spectrum. As seen in the insets of Figs. 7(b) and 7(c), the logarithmic-scale plots of the spectra provide clear evidence that the side-mode suppression ratio is more than 20 dB. A slight redshift of the peak is due to the Joule heating effect of the injection current.

The significant feature of the optical spectra under the cw condition is the single sharp peak observed for a wide range of values of the injection current. The full width at half maximum (FWHM) of the peak is ~0.06 nm, which is close to the resolution limit of 0.05 nm of the optical spectrum analyzer used in this experiment. Additional evidence to support the occurrence of the single-wavelength lasing can be obtained by investigating the existence of the mode-beating signals and the noise enhancement due to multimode fluctuation in the radio-frequency (rf) spectrum of the output light intensity. This detection has been frequently used for lasers with small mode spacing, such as fiber lasers (e.g., see Ref. [34]). In the rf spectrum measurement, we used a fast response photodetector with 3 dB bandwidth, 12.5 GHz. Figure 8 shows the rf spectra of the output intensity for injection current values of $1.3I_{\text{th}}$ and $1.6I_{\text{th}}$. For purposes of comparison, the noise spectrum measured below the threshold current is also shown in the figure. If multimode lasing occurred, the multiple peaks due to the multimode beating could appear in a wide range up to 12.5 GHz [35]. However, the power spectra of the intensity signals do not exhibit any significant enhancement of the intensity noise caused by the multimode beating and fluctuation, although a slight increase of the noise due to the relaxation oscillation can be seen at around 2 GHz. From these results, we conclude that the stadium-shaped laser stably operates at a single wavelength.

C. Far-field pattern

In order to identify the lasing mode, we investigated the far-field emission pattern from the stadium-shaped laser. The far-field pattern was obtained by rotating the photodetector with a slit around the stadium laser. The radius of the rotation and the width of the slit were about 30 cm and 0.5 mm, respectively, which yielded a resolution of 0.1°. In the measurement, we set the collection axis to have a slight angle with respect to

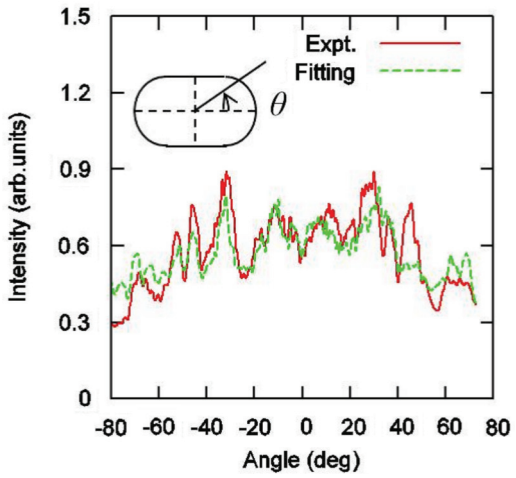

FIG. 9. (Color online) Far-field pattern of the stadium-shaped laser (red solid curve) together with the theoretical curve fitted by using five low-loss cavity modes (green dashed curve).

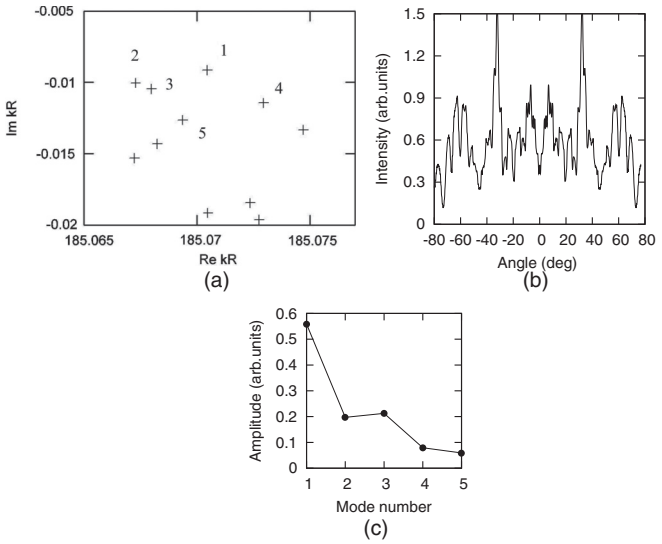

FIG. 10. (a) Distribution of the resonances kR around the lasing wavelength of 848.75 nm. The mode number j(=1,2,3,4,5) is assigned in order from the lowest loss mode. The parities of the modes with respect to the major axis of the stadium are, respectively, even, odd, even, odd, and odd. (b) Far-field pattern of the lowest-loss cavity mode ($j = 1$). (c) The amplitude a_j obtained from the fitting calculation.

the horizontal plane where the laser was placed, taking into account the Lloyd's mirror interference between the output light and the reflected light at the GaAs substrate. The tilt angle was determined so that the output light coupled to the detector maximally.

The measured far-field pattern is shown in Fig. 9, where the pattern is smoothed out by a moving average to display the characteristics more clearly. The temperature and injection current of the laser stabilized to better than $\pm 0.01\,^{\circ}$C and 0.06 mA, respectively. We confirmed that the pattern was stationary and stable for the repeated operation of the laser, and the fluctuation was at most 3% of the measured values.

As shown in Fig. 9, the emission pattern is almost uniform, but has several local peaks, resulting from complex interference of the light field emitted from the stadium-shaped laser. It has been confirmed that the envelope of the pattern can be well explained by a ray-dynamical model based on Snell's and Fresnel's laws [20]. However, the entire emission pattern including the local peaks is asymmetric with respect to the major axis.

At this point, let us numerically verify whether the asymmetric far-field emission pattern is due to the locking phenomenon among the nearly-degenerate cavity modes with different parities, as shown in Sec. II. Here, we assume that the experimentally measured far-field pattern $I_{\mathrm{expt}}(\theta)$ can be fitted by the following far-field pattern $I(\theta)$:

$$I(\theta) = \left| \sum_{j=1}^{N} a_j e^{i\phi_j} \psi_j(\theta) \right|^2 + \beta, \tag{5}$$

which is the superposition of the wave function at infinity $\psi_j(\theta)$ of the cavity modes j ($j = 1,2,\ldots,N$), whose wavelengths are around the measured lasing wavelength of 848.75 nm. In the equation, a_j and ϕ_j denote real amplitude and phase coefficients, respectively, for mode j, and β represents the background level due to the spontaneous emission. The unknown coefficients a_j, ϕ_j, and β are determined such that the following evaluation function J takes the minimum:

$$J[I] = \int_C |I(\theta) - I_{\mathrm{expt}}(\theta)| d\theta, \tag{6}$$

where C denotes the measurement range $C \in [-80,80]$.

The wave functions of the cavity modes can be obtained as the eigensolutions of the Helmholtz equation $[\nabla^2 + n^2 k_j^2]\psi_j = 0$ under outgoing-wave condition at infinity [3], where n is the refractive index. k_j and ψ_j denote the wave number of an eigenvalue and the eigenfunction of the Helmholtz equation, respectively. As mentioned in Sec. II, because of leakage from a cavity, the eigenwave number k_j always becomes complex; the real part of k_j denotes the resonance wave number, while the imaginary part represents the decay rate of the cavity mode.

Figure 10(a) shows the distribution of the dimensionless wave number kR over the range corresponding to the lasing wavelength 848.75 $\pm$ 0.025 nm. In this calculation, the boundary element method was used [30]. The effective refractive index was assumed to be 3.3. We emphasize that this cavity-mode calculation was performed for the real cavity size used in the experiment.

First, for comparison purposes, we used a single cavity mode and carried out the fitting calculation using a Monte Carlo simulation. The best value of $J/J[0]$ we could obtain was 0.33, where $J[0] = \int_C I_{\mathrm{expt}}(\theta) d\theta$. The large mismatch in the fitting is due to the symmetric pattern of the cavity modes and the large amplitude oscillation. As an example, the pattern of the lowest loss mode is shown in Fig. 10(b). The large amplitude oscillation is not a peculiar feature of the cavity mode, but a common feature of all the cavity modes [20].

The value of J can be improved by increasing the number of the modes in the fitting calculation. The far-field pattern obtained from the fitting calculation using five low-loss modes

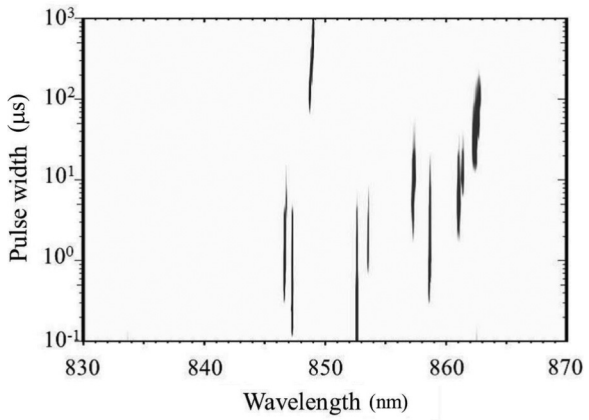

FIG. 11. Pulse width dependence of the optical spectra. The intensity is stronger as the color darkens.

($j = 1, \ldots, 5$) shown in Fig. 10(a) is superimposed with a green dashed curve in Fig. 9. The pattern is asymmetric, and the oscillation amplitude decreases because of the interference among the many cavity modes. The value of $J/J[0]$ is about 0.12, which is three times better than the single-cavity mode. The amplitude of each cavity mode is shown in Fig. 10(c), where the mode number j is labeled from the lowest loss mode in order (e.g., $j = 1$ denotes the lowest loss mode, $j = 2$ denotes the second-lowest loss mode, and so on). We also confirmed that the fitting pattern is almost unchanged even when higher loss modes are taken into account in the fitting calculation. These results suggest that the experimental far-field pattern can be interpreted as that of the locking state among the five low-loss modes. A deviation from the experimental pattern I_{expt} may be attributed to the change in the refractive index upon the current injection, impurities around the laser cavity, and the use of the two-dimensional approximation of the wave functions of the cavity modes.

IV. OPTICAL SPECTRA UNDER PULSED-PUMPING OPERATION

Lastly, we discuss what pumping conditions are necessary for observing the single-wavelength lasing in order to relate our studies with previous experimental works, in which it has been reported that multimode lasing can be observed in stadium-shaped microcavity semiconductor lasers [18,20,23]. For this purpose, we investigated the optical spectra under pulsed-pumping conditions. In this experiment, the width of the pulse current applied to the laser diode was set to be in the range of 0.1–990 μs, while the repetition rate was fixed to be 1 kHz, i.e., the duty cycle was varied from 0.1% to 99%. The maximum and minimum values of the pulse current were fixed as $1.3I_{\text{th}}$ and 0 mA, respectively. The results are summarized in Fig. 11 by a contour plot in the pulse-width and wavelength plane, where the gray-colored scale represents the spectral intensity. We can clearly observe the increase and decrease in the number of lasing modes as the pulse width is changed.

For a short pulse width of 0.1 μs, a single peak around 853 nm, which is close to the maximum of the ASE spectra, is observed. As the pulse width gets longer, the other peaks appear, particularly in the long-wavelength regime around 860 nm. When the pulse width further increases, their peaks are suppressed, while a peak around 849 nm, corresponding to the wavelength observed in the case of cw operation, gradually increases. Finally, only this peak survives, and stable single-wavelength lasing can be observed.

It is important to note that the pulse width is related to the time interval during which the cavity modes are excited. We speculate that the change in the lasing modes from the short pulse to long pulse region is related to the transient dynamical behaviors of the lasing modes toward the single-wavelength lasing state, as numerically demonstrated in Sec. II B 1. When the width of the pumping pulse, i.e., the time of the excitation, is much shorter than a relaxation time to the lasing state, the intensities of each lasing mode are so small that gain competition does not occur among them. Considering that the spectral measurement is carried out for a long time interval, the spectrum reflects the time-averaged intensities of the modes in the early-transient time regime toward the single-wavelength lasing, and thus it can exhibit multiple peaks. As the pulse width is longer, a nonlinear interaction such as gain competition starts to occur, inducing a decrease of the number of lasing modes. Therefore, in the spectrum, the number of peaks is observed to decrease. We speculate that such gain competition can cause a drastic change of dominant lasing modes over a wide range of the wavelengths, as seen in Fig. 11. The deformation of the gain spectrum due to the Joule heating effect of the injection current may also partly contribute to the change.

We note that a long pulse width of over 900 μs (i.e., 90% duty cycle) is needed to achieve a stable single-wavelength lasing in our experiment. The long time scale is partly due to our measurement method, which requires a long time to detect the spectral features. Therefore, the observed pulse-width dependence of the spectrum does not directly reflect the mode dynamics. However, we believe that our approach could be useful for qualitatively understanding a transient dynamical behavior and controlling the lasing states.

V. SUMMARY AND DISCUSSIONS

In summary, we numerically and experimentally investigated the lasing properties of stadium-shaped chaotic microcavity lasers under both cw and pulsed-pumping conditions. The numerical simulation based on the SB model revealed that a stable and stationary single-wavelength lasing is generally observed under cw pumping condition, even when many cavity modes have positive net gain. The emission pattern was found to be asymmetric with respect to a symmetry axis of the stadium-shaped cavity, which was explained as due to the frequency-locking interaction between nearly-degenerate cavity modes with different parities. The interesting point is that the lasing state is formed by the integration of two low-loss modes due to the frequency locking. The spatial pattern is extended to the whole area inside the cavity, which can increase gain competition and suppress the lasing of the other modes.

We observed single-wavelength lasing with asymmetric emission pattern in a semiconductor laser diode with a stadium-shaped cavity under cw condition. We quantitatively confirmed that the observed asymmetric pattern is better fitted

by the superposition of five low-loss cavity modes than by a single cavity mode. On the basis of numerical simulations of the SB model, we considered that such a superposition is due to the frequency-locking effect.

We also experimentally observed that under short pulsed-pumping conditions, multimode lasing is possible. However, the number of lasing modes decreases as the width of the pulse current (i.e., the time of excitation) increases, thereby indicating that after the transient, the stable single-wavelength lasing state can be achieved under long pulsed-pumping condition.

We emphasize that the interpretation of our numerical and experimental results on the single-wavelength lasing is different from those of previous works [25–27], where single-wavelength lasing has been explained with a simple picture based on a single low-loss cavity mode. The asymmetric lasing emission pattern we observed numerically and experimentally cannot be fully explained using such a simple picture. Because the origin of the single-wavelength lasing is the strong modal interaction resulting from the spreading of spatial patterns over the whole cavity area due to wave chaos, as mentioned in Sec. II B3, we expect that single-wavelength lasing can generally be observed for the other chaotic microcavity lasers operated in cw pumping.

ACKNOWLEDGMENT

This work was partially supported by Grant-in-Aid for Young Scientists (B) (Grant No. 10463704), Japan Society for the Promotion of Science.

[1] T. Harayama and S. Shinohara, Laser Photonics Rev. **5**, 247 (2011).
[2] S. L. McCall, A. E. J. Levi, R. E. Slusher, S. J. Pearton, and R. A. Logan, Appl. Phys. Lett. **60**, 289 (1992).
[3] J. U. Nöckel and A. D. Stone, in *Optical Processes in Microcavities*, edited by R. K. Chang and A. J. Campillo, (World Scientific, New York, 1996); Nature (London) **385**, 45 (1997).
[4] C. Gmachl, F. Cappasso, E. E. Narimanov, J. U. Nöckel, A. D. Stone, J. Faist, D. L. Sivco, and A. Y. Cho, Science **280**, 1556 (1998).
[5] G. D. Chern, H. E. Türeci, A. D. Stone, R. K. Chang, M. Kneissl, and N. M. Johnson, Appl. Phys. Lett. **83**, 1710 (2003); M. Kneissl, M. Teepe, N. Miyashita, N. M. Johnson, G. F. Chern, and R. K. Chang, *ibid.* **84**, 2485 (2004).
[6] J. Wiersig and M. Hentschel, Phys. Rev. Lett. **100**, 033901 (2008); C. Yan, Q. J. Wang, L. Diehl, M. Hentschel, J. Wiersig, N. Yu, C. Pflügl, F. Capasso, M. A. Belkin, T. Edamura, M. Yamanishi, and H. Kan, Appl. Phys. Lett. **94**, 251101 (2009); Q. Song, W. Fang, B. Liu, S.-T. Ho, G. S. Solomon, and H. Cao, Phys. Rev. A **80**, 041807(R) (2009).
[7] K. J. Vahala, Nature (London) **424**, 839 (2003).
[8] H. E. Türeci, A. D. Stone, and B. Collier, Phys. Rev. A **74**, 043822 (2006).
[9] E. Bogomolny, N. Djellali, R. Dubertrand, I. Gozhyk, M. Lebental, C. Schmit, C. Ulysse, and J. Zyss, Phys. Rev. E **83**, 036208 (2011); E. Bogomolny, R. Dubertrand, and C. Schmit, *ibid.* **78**, 056202 (2008).
[10] J. W. Ryu, S. Y. Lee, C. M. Kim, and Y. J. Park, Phys. Rev. E **73**, 036207 (2006); S. Shinohara and T. Harayama, *ibid.* **75**, 036216 (2007).
[11] T. Fukushima, T. Harayama, and J. Wiersig, Phys. Rev. A **73**, 023816 (2006).
[12] S. Y. Lee, S. Rim, J. W. Ryu, T. Y. Kwon, M. Choi, and C. M. Kim, Phys. Rev. Lett. **93**, 164102 (2004).
[13] T. Harayama, P. Davis, and K. S. Ikeda, Phys. Rev. Lett. **90**, 063901 (2003).
[14] T. Harayama, T. Fukushima, S. Sunada, and K. S. Ikeda, Phys. Rev. Lett. **91**, 073903 (2003).
[15] S. Sunada, T. Harayama, and K. S. Ikeda, Phys. Rev. E **71**, 046209 (2005).
[16] T. Harayama, S. Sunada, and K. S. Ikeda, Phys. Rev. A **72**, 013803 (2005).
[17] S. Shinohara, T. Harayama, H. E. Türeci, and A. D. Stone, Phys. Rev. A **74**, 033820 (2006).
[18] T. Fukushima and T. Harayama, IEEE J. Sel. Top. Quantum Electron. **10**, 1039 (2004).
[19] T. Harayama, T. Fukushima, P. Davis, P. O. Vaccaro, T. Miyasaka, T. Nishimura, and T. Aida, Phys. Rev. E **67**, 015207 (2003).
[20] S. Shinohara, T. Fukushima, and T. Harayama, Phys. Rev. A **77**, 033807 (2008).
[21] M. Lebental, J. S. Laurel, R. Hierle, and J. Zyss, Appl. Phys. Lett. **88**, 031108 (2006).
[22] M. Lebental, J. S. Lauret, J. Zyss, C. Schmit, and E. Bogomolny, Phys. Rev. A **75**, 033806 (2007).
[23] M. Choi, S. Shinohara, and T. Harayama, Opt. Express **16**, 17554 (2008).
[24] W. Fang, H. Cao, and G. S. Solomon, Appl. Phys. Lett. **90**, 081108 (2007).
[25] R. Audet, M. A. Belkin, J. A. Fan, B. G. Lee, K. Lin, F. Capasso, E. E. Narimanov, D. Bour, S. Corzine, J. Zhu, and G. Höfler, Appl. Phys. Lett. **91**, 131106 (2007).
[26] M.-W. Kim, C.-H. Yi, S. Rim, C.-M. Kim, J.-H. Kim, and K.-R. Oh, Opt. Express **20**, 13651 (2012).
[27] T. Fukushima, T. Tanaka, and T. Harayama, Opt. Lett. **32**, 3397 (2007).
[28] H. E. Türeci, L. Ge, S. Rotter, and A. D. Stone, Science **320**, 643 (2008).
[29] P. Stano and P. Jacquod, Nat. Photonics **7**, 66 (2013).
[30] J. Wiersig, J. Opt. A: Pure Appl. Opt. **5**, 53 (2003).
[31] S. Sunada, T. Harayama, and K. S. Ikeda, Nonlinear Phenom. Complex Syst. (Dordrecht, Neth.) **10**, 1 (2007).
[32] The spatial overlap between the two modes, which is characterized as $\langle|\psi_{++}|^2|\psi_{-+}|^2\rangle/\sqrt{\langle|\psi_{++}|^4\rangle\langle|\psi_{-+}|^4\rangle}$, is about 0.4, where $\langle\cdots\rangle$ denotes the spatial integration inside the cavity area.
[33] X. Jiang and C. M. Soukoulis, Phys. Rev. Lett. **85**, 70 (2000).
[34] K. Inagaki, S. Tamura, T. Tanaka, H. Noto, and T. Harayama, Proc. SPIE **7004**, 70045F (2008).
[35] The range of the beat frequency measurement can be estimated from the cavity-mode calculation, because the beat frequency is similar to the mode spacing for the stadium cavity.